Published in final edited form as:
Phys Med Biol. 2012 December 7; 57(23): 8061–8078. doi:10.1088/0031-9155/57/23/8061.

Ultrasonic atomization of tissue and its role in tissue fractionation by high intensity focused ultrasound

Julianna C. Simon[1], **Oleg A. Sapozhnikov**[1,2], **Vera A. Khokhlova**[1,2], **Yak-Nam Wang**[1], **Lawrence A. Crum**[1], and **Michael R. Bailey**[1]

Julianna C. Simon: jcsimon@uw.edu; Oleg A. Sapozhnikov: olegs@apl.washington.edu; Vera A. Khokhlova: vera@apl.washington.edu; Yak-Nam Wang: ynwang@apl.washington.edu; Lawrence A. Crum: lac@apl.washington.edu; Michael R. Bailey: bailey@apl.washington.edu

[1]Center for Industrial and Medical Ultrasound, Applied Physics Laboratory, University of Washington, 1013 NE 40th Street, Seattle, WA 98105, USA

[2]Department of Acoustics, Physics Faculty, Moscow State University, Leninskie Gory, Moscow 119991, Russia

Abstract

Atomization and fountain formation is a well-known phenomenon that occurs when a focused ultrasound wave in liquid encounters an air interface. High intensity focused ultrasound (HIFU) has been shown to fractionate tissue into submicron-size fragments in a process termed boiling histotripsy, wherein the focused ultrasound wave superheats the tissue at the focus, producing a millimetre-size boiling or vapour bubble in several milliseconds. Yet the question of how this millimetre-size boiling bubble creates submicron-size tissue fragments remains. The hypothesis of this work is that tissue can behave as a liquid such that it forms a fountain and atomization within the vapour bubble produced in boiling histotripsy. We describe an experiment, in which a 2-MHz HIFU transducer (maximum *in situ* intensity of 24,000 W/cm^2) was aligned with an air-tissue interface meant to simulate the boiling bubble. Atomization and fountain formation were observed with high-speed photography and resulted in tissue erosion. Histological examination of the atomized tissue showed whole and fragmented cells and nuclei. Air-liquid interfaces were also filmed. Our conclusion was that HIFU can fountain and atomize tissue. Although this process does not entirely mimic what was observed in liquids, it does explain many aspects of tissue fractionation in boiling histotripsy.

Keywords

Atomization; fountain; high intensity focused ultrasound; HIFU; histotripsy

1. Introduction

Ultrasonic atomization, or the emission of droplets from an acoustically excited thin liquid film exposed to air, was first reported by Wood and Loomis (1927). More recently, McCubbin (1953) investigated the size of the droplets in the fog produced in a fountain formed by focused ultrasound. Since then, ultrasonic atomization has been the basis for many air humidifiers and medical nebulizers and has been proposed to play a role in tissue injury in the lungs by medical ultrasound (Tjan and Phillips 2007, 2008). The hypothesis of this work is that atomization and fountain formation by high intensity focused ultrasound (HIFU) occurs similarly in liquids and tissues. A further hypothesis is that tissue fractionation by HIFU is a result of atomization and fountain formation. This paper reports experimental observations of these phenomena for planar interfaces of liquid-air and tissue-

air. In addition, fountain formation and atomization of tissue for small gas cavities are also examined.

Acoustic atomization has been described by both cavitation and capillary-wave theories (Rozenberg 1973). Söllner (1936) conducted a series of experiments in liquids of varying viscosity under low pressure and elevated temperature conditions and concluded that atomization is caused by the violent collapse of bubbles. However, Bisa, Dirnagl, and Esche proposed a capillary-wave hypothesis based on their experimental observations of the particle size distribution from the atomization of various liquids in a fountain (Rozenberg and Éknadiosyants 1960, Gershenzon and Éknadiosyants 1964). In the capillary-wave hypothesis, a liquid is parametrically excited such that capillary waves are formed on the surface at one-half the excitation frequency (Faraday 1831, Rozenberg 1973). As the amplitude of these waves increase, the waves become instable and small droplets pinch off from the crests causing atomization (Gershenzon and Éknadiosyants 1964). Additional experimental evidence published by Lang (1962), showed a strong relationship between ultrasonic frequency and droplet diameter, further supporting the capillary-wave theory of ultrasonic atomization. Theoretical studies began to emerge, most notably by Peskin and Raco (1963), who completed a stability analysis of the hydrodynamic equations for planar ultrasound waves, and showed that a constant relationship existed between the mean droplet diameter and the capillary wavelength. Yet, Antonevich (1959) concluded, based on high-speed experimental observations for low frequency planar ultrasound waves, that atomization was a combination of cavitation bubble collapse and capillary wave instabilities, and that the size of the emitted droplets depended upon the ejection mechanism. Several iterations of the cavitation-wave hypothesis, a combination of the cavitation and capillary wave hypotheses, emerged to explain the mechanism for atomization of liquids in a fountain (Boguslavskii and Éknadiosyants 1969, Rozenberg 1973). One interpretation of the cavitation-wave hypothesis is that radiation force from the focused wave causes bulging of the liquid surface, focusing the waves inverted by the pressure release interface, and causing the formation of numerous cavitation bubbles in the bulging volume of liquid. Oscillation and collapses of these cavitation bubbles enhance microscale surface perturbations and thus facilitate the pinch-off of droplets, *i.e.,* atomization. While none of these three hypotheses (cavitation, capillary wave, cavitation-wave) has been completely accepted, a version of the cavitation-wave hypothesis appears to describe most accurately what is observed in liquid fountains formed by focused ultrasound (Topp 1973, Bassett and Bright 1976, Barreras *et al.* 2002).

HIFU has been used clinically to thermally coagulate tissue in a well-defined focal volume (ter Haar 2001, Bailey *et al.* 2003). An alternative to tissue denaturation, HIFU has also been shown be able to cut through the heart septum (Smith and Hynynen 1998) and to fractionate tissue by pulsed ultrasound cavitation or shock wave heating and millisecond boiling (Parsons *et al.* 2006, Maxwell *et al.* 2011, Canney *et al.* 2010a, Khokhlova *et al.* 2011a). Histotripsy, or pulsed ultrasound cavitation therapy, uses microsecond pulses at high pulse-repetition frequencies (PRFs) and acoustic pressures (peak positive pressure (p_+) of $p_+ >$ 80MPa and peak negative pressure (p_-) of $p_- < -20$ MPa in water) to maintain a cavitation bubble cloud on the order of several millimetres in size, composed of bubbles on the order of hundreds of microns in diameter, which homogenizes the tissue at the focal zone (Parsons *et al.* 2006, Maxwell *et al.* 2011, Wang *et al.* 2012). On the other hand, shock wave heating and millisecond boiling, hereafter denoted as boiling histotripsy, uses millisecond pulses, low PRFs, and lower acoustic pressures than cavitation cloud histotripsy (peak pressures of $p_+ > 40$ MPa and $p_- = -10$ MPa in water) to explosively expand a millimetre-size boiling bubble at the focus to fractionate tissue (Canney *et al.* 2010a, Khokhlova *et al.* 2011a). The end results of cavitation and boiling histotrispy are submicron-size tissue fragments (Parsons

et al. 2006, Wang *et al.* 2011); however, it is unclear how large boiling bubbles or cavitation bubble clouds can create submicron-size tissue pieces.

The goal of this paper is to present experimental evidence that acoustic atomization and fountain formation together form a possible mechanism by which the large, millimetre-size bubbles in boiling histotripsy produce submicron-size tissue fragments. To compare liquid and tissue fountains and atomization, flat interfaces between air and either a liquid or tissue were exposed to HIFU and filmed with high-speed videography. By modifying HIFU amplitudes, timing protocols, and number of pulses, the thresholds of atomization were established for several tissues and fluids. To relate to boiling histotripsy, the possibility of atomization within a millimetre-diameter tissue-air interface was established. At the end of each exposure, the dimensions of the resulting crater were measured and the volume of eroded tissue was calculated. An important result is an experimentally-tested mechanism of tissue fractionation by HIFU, which may lead to safer and more efficient tissue homogenization as the techniques move to the clinical regime.

2. Methods

Figure 1 illustrates the proposed mechanism of tissue fractionation in boiling histotripsy. As was shown previously, the tissue at the focus is heated rapidly, such that a millimetre-size boiling bubble is formed at the transducer focus in a predictable time (Canney *et al.* 2010a); however, it is unclear how the millimetre-size boiling bubble can produce submicron-size tissue fragments (Khokhlova *et al.* 2011a). Some suggested mechanisms of tissue fractionation include explosive growth of a boiling bubble and tissue spallation due to reflection of a shock wave from the boiling bubble or bubble cloud with corresponding increases in negative pressure close to the interface (Maxwell *et al.* 2011, Khokhlova *et al.* 2011a). The idea proposed here is that the vapour-filled boiling bubble will be of sufficient size to act as a pressure-release interface, such that a miniature acoustic fountain will form and atomization will occur within the boiling bubble. In addition, atomization will be the process by which the large boiling bubble fractionates the tissue into submicron-size fragments. To experimentally test whether reflection from the bubble is similar to reflection from a flat pressure-release interface, a cylindrical hole will be bored through tissue. While the cylindrical hole is not equivalent to the spherical bubble created by boiling histotripsy in bulk tissue, the hole allows for observation while maintaining a similar curvature in 2 dimensions as the boiling bubble shows in 3 dimensions. To reiterate, these experiments will begin with an existing void that simulates the void made by boiling in the more clinical case (*i.e.,* in bulk tissue). Then, as with the boiling histotripsy case, the void will continue to be insonified and the interaction between the focused sound and the void will fractionate the tissue.

2.1. Acoustic characterization and exposures

For all experiments, the ultrasound transducer used was an air-backed, single-element, spherically focused piezoceramic crystal (PZ 26, Ferroperm Piezoceramics, Kvistgaard, Denmark), with an operational frequency of 2.165 MHz mounted in custom-built polycarbonate housing. A function generator (Model 33250A, Agilent, Palo Alto, CA, USA) and a linear radiofrequency (RF) amplifier (55 dB Gain, Model A300, ENI, Rochester, NY, USA) were used to drive the transducer. The diameter and radius of curvature of the transducer was 45 mm. Before the experiments, a fibre-optic probe hydrophone (FOPH 2000, RP Acoustics, Leutenbach, Germany) with 100-μm active diameter was used to measure the focal pressure waveform in water. A similar transducer, with slightly different operational frequency and housing, was thoroughly characterized in Canney *et al.* (2008) and used in previous boiling histotripsy studies (Canney *et al.* 2010a, Khokhlova *et al.* 2011a).

Measurements were conducted in filtered and degassed room temperature (~20° C) water at increasing power outputs. A force balance was built in-house with a brush absorber, an Acculab VI-3mg scale (Columbia, MD, USA), and was controlled with Labview (National Instruments, Austin, TX, USA) programming. The measurements were conducted to ensure that power increased quadratically with voltage. Peak positive and peak negative pressures were obtained from pressure waveforms measured at the focus; focal intensities (I_L) were linearly scaled from low output measurements (Canney *et al.* 2008) and are reported in figure 2. The maximum acoustic output of the transducer in water (figure 2) corresponds to an intensity at the focus of approximately $I_L = 24{,}000$ W/cm^2, with $p_+ = 65$ MPa and $p_- = 16$ MPa.

These measurements in water were translated into tissue using the previously developed derating methods for nonlinear high intensity focused ultrasound waves (Bessonova *et al.* 2010, Canney *et al.* 2010a, Khokhlova *et al.* 2011a). Briefly, the *in situ* intensities and peak pressures at the focus in tissue for a given output of the transducer corresponded to those measured in water for some lower power output. The scaling factor between outputs was calculated as $\exp(-2\alpha L)$, where α is the attenuation coefficient in tissue at the operational frequency of the transducer and L is the tissue depth. As has been shown in previous studies, when the source outputs are scaled to account for linear attenuation losses in tissue, then both the peak pressure levels and intensity at the focus as well as the degree of nonlinear waveform distortion are similar in water and tissue (Bessonova *et al.* 2010, Canney *et al.* 2010a, Khokhlova *et al.* 2011a). Figure 2 shows the waveforms corresponding to the various experimental conditions.

For this study, an exposure consisted of one or several 10-ms pulses repeated at a 1 Hz pulse repetition frequency as in the previous boiling histotripsy studies (Khokhlova *et al.* 2011a). All experiments were conducted at room temperature (~20°C) with water filtered to remove particulates larger than 5 μm and degassed with a Liqui-Cel Extra-Flow 2.5 × 8 gas contactor membrane with ×50 fiber (Membrana, Charlotte, NC, USA) to less than 20% of saturation as measured with a dissolved oxygen meter (WTW Oxi 330i, Weilheim, Germany).

2.2. Experiments with planar interface

The experimental arrangement for interrogation of liquids or flat tissue interfaces at the macro scale is displayed in figure 3(a). One goal of these experiments was to better understand the role of cavitation in the atomization of liquid fountains. Previously, researchers have considered the role of cavitation through sonoluminescence and the manipulation of ambient pressure, transducer frequency, temperature, surface tension, and viscosity (Söllner 1936, Rozenberg and Éknadiosyants 1960, Gershenzon and Éknadiosyants 1964, Il'in and Éknadiosyants 1967, Il'in and Éknadiosyants 1969). A reprise of those studies was conducted with a focus on manipulating the shear viscosity of the liquid using the experimental arrangement shown in figure 3(a). Water (shear viscosity 0.0009 Pa s), ethanol (0.001 Pa s), castor oil (0.99 Pa s), and glycerol (1.2 Pa s) were placed at the focus of the transducer and filmed with a Photron APX-RS high speed camera (monochrome, Photron, San Diego, CA, USA). The liquid was held in a custom-designed container with an acoustically transparent, thin plastic film bottom. The container was placed in water such that the bottom of the container was positioned just below the water surface. The thickness of the liquid layer was variable between 2–15 millimetres. The transducer was focused at the liquid surface using pulse echo with the timing recorded on a digital oscilloscope (Model LT432, Lecroy, Chestnut Ridge, NY, UA). The Photron high-speed camera was operated at 20,000 frames per second with a resolution of 256×512 pixels. A Carl Zeiss lens (Makro-Planar T* 2/100, Thornwood, NY, USA) with a bellows extension was used to provide a resolution on the order of 40 μm/pixel. A continuous, disperse light source (Photogenic

PowerLight 2500DR, Bartlett, IL, USA) positioned at an angle slightly off axis from the camera lens was used to backlight the liquid to air interface.

To directly compare atomization in tissue with that in the liquids, the same macro setup as shown in figure 3(a) was used. The tissue was held in a similar plastic holder as the liquids without the plastic film. To fit the container, the tissue was cut into pieces approximately 5.5 cm × 5.5 cm with a depth varying between 1 cm and 1.5 cm. All equipment used to drive the function generator and to film the event was described in the previous paragraph.

2.3. Experiments with bubble-mimicking interface

Figure 3(b) shows the experimental arrangement used to determine if tissue would atomize at a curved, millimetre-size, bubble-like interface. The same camera and acoustic equipment were used as has been described above; however, the tissue was prepared and held differently. The tissue was sectioned into samples approximately 8 cm × 8 cm × 2.5 cm and mounted into a custom-made holder that would suspend the tissue without interference to the acoustic field. Biopsy punches of 1–3 mm diameter were used to bore through the 2.5 cm of tissue at a position approximately 1.5 cm from the bottom surface of the tissue, creating a cylindrical tunnel. The transducer was focused at the bottom surface of the cylindrical tunnel using the pulse-echo technique.

2.4. Experiments with micro tissue setup

To examine the contents of the jet more thoroughly, and to obtain a more precise estimate of the commencement time for atomization, a micro setup was used as is illustrated in figure 4. With the tissue surface under interrogation placed parallel to gravity, the surface was filmed through an inverted microscope (TE2000-U, Nikon Inc., Melville, NY, USA) with the Imacon 200 ultra-high-speed camera (DRS Hadland, Cupertino, CA, USA). The experiment was backlit with a fibre optic illuminator (Model 41500-50, Cole-Parmer Instrument Co., Vernon Hills, IL, USA) positioned just in front of the tissue surface. The transducer was driven by a function generator (Model AFG3022B, Tektronix, Beaverton, OR, USA) and a linear RF amplifier (55 dB Gain, Model A150, ENI, Rochester, NY, USA). Because of space constraints, the transducer was positioned at 45° with respect to the tissue surface. As before, the transducer was focused at the surface using the pulse echo technique. For this experimental arrangement, the tissue was sectioned into samples of approximately 8 cm × 3 cm with a depth of 1 cm and placed under tension in a custom-designed tissue holder.

2.5. Tissue preparation and analysis

Two different biological samples were used in these experiments: bovine liver and porcine blood clot.

Bovine liver was purchased from a local abattoir (Schenk Packing, Stanwood, WA, USA) and used within 8 hours of harvesting. The liver was kept on ice until arrival at the lab, where it was cut into the sizes specified for each experimental arrangement, taking care not to include blood vessels in the sample. The liver capsule was not present on the interrogated surface and surface imperfections such as vessels and kerf marks were avoided. After cutting, the liver was immersed in phosphate buffered saline (PBS) and degassed for approximately one hour on ice in a desiccant chamber of −85 kPa. For nonlinear derating calculations in liver, the attenuation coefficient used was α=0.7 dB/cm/MHz (Canney *et al.* 2010a).

Porcine blood clots were exposed to the experimental conditions as an intermediary between tissue and liquids. Blood was collected from a terminal porcine study conducted at the University of Washington and then placed in a holder and allowed to clot for approximately

one hour at room temperature. Once the clot had formed, it was moved to the custom-designed holder described previously for the flat macro setup shown in figure 3(a). For nonlinear derating calculations in blood clots, the attenuation coefficient used was α=0.93 dB/cm/MHz (Nahirnyak *et al.* 2006).

Sizes of the emitted droplets and distances between jets were calculated from analysis of the high speed videos. In addition, calipers were used to measure, to the nearest half-millimeter, the erosion depth along with the horizontal and vertical diameters (with respect to the tissue piece) for the planar interface (figure 3(a)). The volume of eroded tissue was calculated assuming the eroded volume has approximately the shape of a spherical cap. Furthermore, fountained and atomized tissue projectiles were collected from the micro setup by placing a glass slide beneath the fountain location. The collected projectiles were allowed to dry on the slide, stained with Haematoxylin and Eosin (H&E), and visualized by light microscopy.

3. Results

3.1. Planar interface

As was previously observed in water (Rozenberg and Éknadiosyants 1960, Il'in and Éknadiosyants 1967), for low acoustic intensities (I_L=180 W/cm^2; $p_+ = 2.5$ MPa, $p_- = 2$ MPa) at which atomization only occurs intermittently in water, the fountain is a chain of drops and one or more drops explode (*i.e.,* atomize) as shown in figure 5(a). While for this case, atomization occurred 2.65 ms into the pulse, in general, atomization does not occur in a predictable time at these intensities. The sizes of the individual droplets within the emitted jets are mostly less than a few microns, though a few droplets reach up to 600 μm in diameter. In the sequence of images in figure 5(a), the drop becomes opaque 50 μs before the jets are emitted in a triangular pattern at a velocity of approximately 12 m/s. Such an explosive behaviour of the droplet is discussed later in the Discussion section. When water is exchanged for high viscosity liquids such as castor oil and glycerol (not shown), the drop-chain fountain forms but atomization does not occur, even for very thin layers (~2 mm thick) and maximum acoustic intensities. In 70% ethanol, which has a viscosity approximately equal to that of water but one-third of the surface tension (72 mN/m in water and 22 mN/m in ethanol), atomization occurs relatively similarly to water; at the 180 W/cm^2 intensity in ethanol, there are a few relatively large droplets ejected on the order of 200 μm in diameter at velocities of approximately 2 m/s. As expected, the overall size of droplets in ethanol is much larger than in water and is accompanied by a corresponding decrease in velocity.

At the maximum focal acoustic intensity in water ($I_L = 24{,}000$ W/cm^2) cavitation bubbles appear beneath the surface of the water immediately before the violent ejection of droplets from the surface as shown in figure 5(b). Standing waves can also be observed in the water beneath the pressure-release interface (figure 5(b), frames 1–4). At this intensity, atomization, or the emission of fine droplets from the surface, occurs almost instantaneously, approximately 2 μs after the acoustic wave arrives at the interface. The jet velocity is approximately 11 m/s, which is on the same order as the jet velocity observed previously at very low intensities. In 70% ethanol at maximum intensity, atomization occurs in a similar time frame as was observed in water; however, the jet velocity is approximately double, with jet velocities of initial atomization events reaching 25 m/s. As expected, the fountain heights in water depend on the acoustic intensity; the low amplitude fountain height is on the order of a few centimetres, while the high intensity fountain reaches the ceiling of the room positioned about 2 meters above the liquid surface. These observations of fountain formation and the commencement (or lack) of atomization in liquids of varying viscosity or with different levels of acoustic intensity concur with the lack of atomization seen by previous researchers upon increasing the static pressure or lowering the gas content in the

liquid (Söllner 1936, Éknadiosyants 1968, Il'in and Éknadiosyants 1969), which underlines the importance of cavitation in the inception of atomization.

Relating the observations from liquids to tissue, figure 6 depicts bovine liver and water at intensities just above their respective thresholds (I_L = 8,100 W/cm^2; p_+ = 35 MPa, p_- = 9.2 MPa derated in liver, I_L = 550 W/cm^2; p_+ = 5.5 MPa, p_- = 4 MPa in water) where atomization occurs in a relatively repeatable manner. Upon comparison of the two image sequences, it was evident that the free liver surface only partly mimicked the behaviour of water. In liver, an initial small volume of fine spray was ejected from the flat liver surface shortly before the tissue started to bulge. As the acoustic pulse continued, the tissue mound became more distinct and more jets emerged, primarily from the top surface of the mound. In the course of one 10-ms pulse, the mound of liver reached 1.5 mm in height. The jets ejected from the liver surface ranged in size from a few microns up to several hundred microns in diameter, with velocities of approximately 13 m/s, although some of the initial jets reached velocities of 23 m/s. At this intensity, atomization began less than 70 μs after the acoustic wavefront arrived at the interface; however when the derated intensity at the focus was increased to the maximum of 14,000 W/cm^2, atomization was observable a minimum of 20 μs after the wavefront arrived at the surface (supplement 3). With each 10-ms pulse over the course of five pulses repeated at 1 Hz, atomization in liver becomes more dramatic, with an increasing number of jets being emitted from the surface. Conversely, in water (as shown in figure 6 (lower)) a fountain emerged first with a semblance of the drop-chain structure that was observed at lower intensities (figure 5(a)), but with no atomization events occurring until the fountain was fully formed. As the water fountain propagated upwards, a few small atomization events occurred, the first of which was depicted in the third frame at 3.2 ms. However, once the first significant droplet collapse occurred, the fountain quickly degenerated into full-fledged atomization with jets emitted from the sides of the fountain. Interestingly, the jets from the side of the water fountain always emerged from a minimum of 1.2 millimetres above the surface of the water. Similar to liver, the velocity of the fine spray in water was approximately 12 m/s, with the droplets ejected from the water fountain varying in size from a few microns up to several hundred microns in diameter. A qualitative comparison between liver and water showed the number of jets ejected from the water fountain greatly exceeded the number of jets ejected from the tissue fountain; however, in both cases, the formation of the mound substantially increased the number of emitted jets.

In an attempt to reconcile the differences observed between the tissue and liquid fountains, blood clots were exposed to HIFU as an intermediary between tissue and liquid; blood clots form a protein network of fibrin without the structural proteins such as collagen and elastin that are present in tissues (Silverthorn 2004). Figure 7 shows a blood clot exposed to I_L = 1000 W/cm^2 (p_+ = 8.7 MPa, p_- = 5.2 MPa) derated, an intensity above the atomization threshold. Here, the formation of the fountain looks like a hybrid between liver and water at intensities just above their respective atomization thresholds. A combination of liquid and tissue fountain structures emerge; a drop chain formed well into the acoustic pulse (as was observed in the water fountain) from the top surface of a 0.4-mm high mound (similar to what was observed in the tissue fountain). The top droplet extended 1.5 mm above the surface of the blood clot after which the entire droplet detached from the blood clot. Jets were ejected from the blood clot at velocities of approximately 10 m/s. At these intensities, the initial spurt of atomization occurred more than 20 μs after the ultrasonic wave arrived at the interface. As in tissue, a short abatement of atomization occurred after the initial atomization spurt; once the mound formed, more significant atomization ensued. The initial spurt of atomization and the slight pause is thought to be due to excess liquid on the surface of the tissue, even though the tissue is carefully blotted with a paper towel before the exposure. The increase in atomization after the mound forms is likely due to the focusing of

the waves reflected from the pressure release surface and the resulting increase in cavitation below the tissue surface. Table 1 summarizes the quantitative descriptors of some of the different materials placed at the focus of the transducer.

3.2. Bubble-mimicking interface

Before atomization could be proposed as a mechanism for boiling histotripsy, it was necessary to show that the millimetre-size boiling bubble created by boiling histotripsy was large enough to act as a pressure-release interface similar to that seen when the planar tissue was interfaced with air (as in figure 5(a)). Figure 8 shows atomization and fountain formation in a cylindrical, 2-dimensional bubble-like tunnel created in bovine liver at the maximum derated acoustic intensity of I_L = 14,000 W/cm^2 (p_+ = 53 MPa, p_- = 12.7 MPa). The size of the ejected fragments of a few microns up to several hundred microns in diameter and temporal progression of atomization were similar to what was seen with the flat liver-air interface. Jet velocities ranged from approximately 7.5 m/s for small, thicker jets up to 20 m/s for the long, thin, intermittently-released jets. Less than 5 ms into the 10-ms pulse, the 1.5-mm diameter hole became occluded due to the formation of the tissue mound from the radiation force and the size and number of jets emitted from the tissue-air surface. Some pitting of the tissue was observed on the top surface of the hole, most likely due to the violent collision of the jets emitted from the lower surface and the top tissue surface. In addition, tissue erosion was observable on the lower surface of the cylindrical hole similar to what was seen on the flat tissue surface (see figure 9).

3.3 Tissue fractionation

Thus far, it has been shown that atomization of tissue can occur; however, no evidence has been given that atomization of tissue results in the tissue fractionation that was observed in histotripsy and boiling histotripsy studies (Parsons et al. 2006, Canney et al. 2010b, Khokhlova et al. 2011a). Figure 9 shows erosion in a flat liver tissue surface from a varying number of 10-ms pulses at 1 Hz pulse repetition frequency. From the graph of erosion rate over time, it appears as if the volume of the hole is approaching saturation shortly after the number of 10-ms pulses exceeds 300. From the image of the tissue surface, it also appears that the surface dimensions (transverse to the ultrasound pulse direction) approaches saturation around 180 pulses; however from many experiments it was found that the depth of the hole continued to increase even up to 300 pulses and likely beyond, increasing the volume of eroded tissue. An overall erosion rate per 10-ms pulse was calculated to be approximately 0.15±0.07 mm3/10-ms pulse.

In order to look at the contents of the jets, the micro-setup described in figure 4 was used. Figure 10 shows two frames of a magnified view of several jets being emitted from the planar surface of bovine liver (I_L = 7100 W/cm^2 (derated); p_+ = 34 MPa, p_- = 8 MPa). From these images, it is clear that there is a large variation in the diameter of the jets. It is also evident in the jets on the left side of the frames that a fog is emitted (140 μs) slightly before the jet forms (260 μs), which is typical in the formation of jets. Sometimes, jets combine from several smaller jets to produce a large jet, which is present on the left side of each frame. In addition, in the 260-μs frame, a fog is observed between the two mature jets, which may indicate the beginnings of new jets. The presence of several jets in the magnified frames is commonly observed. When the distance between jets is measured over many samples, an average centre-to-centre inter-jet distance emerges of 182±80 μm, which may be indicative of capillary waves on the tissue surface and could help elucidate the overall mechanism of tissue fractionation. Furthermore, upon close examination of the left jet in the 260-μs frame, dark lines are observed within the jet. While this may just be due to light refraction, it could also be evidence of bubbles or eroded tissue within the jet.

The jet contents were collected by placing a microscope slide directly beneath the fountain location in the micro-setup. An H&E stain of the fountain projectiles is shown in figure 11. This section contains whole and disrupted cells and nuclei. Cell clusters are often present, as is visible in the centre of figure 11. Although these cells appear structurally intact, some of the nuclei show evidence of nuclear fading (karyolysis) indicating some damage. Dying single cells (black dashed circles) often show evidence of cell membrane disruption, chromatin condensation (pyknosis) and nuclear fragmentation (karyorrhexis). Red blood cells (white arrowheads) are also present. In addition, the insert shows an example of nuclear disruption and fragmentation (black arrowheads in the insert) that was observed throughout the sample. The presence of cells and nuclei was different from what was observed in histology of cavitation cloud histotripsy in bulk tissue, or for the same conditions used in the free tissue interface scenario (10-ms pulse, 1 Hz PRF) in boiling histotripsy of bulk tissue, where the cells and nuclei were completely homogenized such that no intact cells or nuclei remained (Parsons *et al.* 2006, Wang *et al.* 2011). In addition, bubbles were found in many of the collected projectiles (black arrows), which could help elucidate the role of bubbles in tissue atomization. Modifying the pulse parameters, such as pulse repetition frequency, pulse length (down to 100 μs), and number of pulses did not significantly affect the appearance of whole cells and nuclei within the collected projectiles. The histological differences between atomization of a free tissue interface and bulk histotripsy, both cavitation cloud and boiling, need to be reconciled.

4. Discussion and conclusions

The primary results from this study are that the application of HIFU to a tissue surface can result in the formation of a fountain, which can be atomized, and that the result of this atomization is tissue erosion. However, tissue atomization and fountain formation does not entirely mimic what is typically seen in liquids. Tested parameters include: the acoustic threshold for atomization, the time for atomization to start, and the velocity of the emitted jets. As expected, the threshold for bovine liver atomization is much higher than in water and porcine blood clots (see table 1). Velocities of the projectiles are similar across all the species tested here that atomize and is on the order of 10 m/s. Furthermore, at the maximum intensity in water of 24,000 W/cm^2, atomization begins in microseconds.

An additional result of this study is that there is considerable evidence that tissue atomization and fountain formation is the mechanism by which tissue is fractionated in bulk tissue during boiling histotripsy. It is also possible that it might explain how cavitation histotripsy produces tissue emulsification within the 100 μm-size bubbles or within the cloud of bubbles. While we reported the threshold of atomization in liver in one 10-ms pulse (I_L = 6200 W/cm^2; p_+ = 25 MPa, p_- = 8 MPa), we have also observed atomization in liver after many 10-ms pulses at even lower derated intensities down to I_L = 1300 W/cm^2 (p_+ = 9.5 MPa, p_- = 5.5 MPa). Furthermore, it may be possible to extend the results from this study to diagnostic levels; these results seem to support the hypothesis proposed by Tjian and Phillips (2007, 2008) that atomization is the mechanism by which diagnostic ultrasound can damage lungs, a natural pressure-release interface that occurs in the body. By understanding the mechanism of tissue atomization, a means to protect the lungs may be devised so that ultrasound can be used to scan near the lungs without fear of causing tissue damage.

The explosive behaviour of the droplet shown in figure 5(a) is a result of instabilities caused by the acoustical excitation of the droplet. When the droplet is formed, at some stage it becomes disconnected (or only slightly connected) from the neighbouring droplets in the chain. Note that such a droplet becomes a highly excited spherical acoustic resonator because it has taken a portion of the acoustic energy that was initially in the fountain.

Studies on the free oscillations of liquid droplets began more than one hundred years ago, first by Kelvin (1890) then Rayleigh (1894). Oscillations of liquid drops are of interest in many areas of science, *e.g.,* in chemical engineering; raindrop behaviour is important in cloud physics. It is known that drop oscillation can become unstable; when nonspherical deformations of the drop shape develop, the drop can be broken into pieces. These instabilities are one possible reason for the observed explosion of droplets in a fountain. Another possible reason is that cavitation may occur inside the droplet that is oscillating radially (in a "breathing" mode). Such cavitation most probably starts in the centre of the droplet, where the standing acoustic wave is at maximum amplitude. Before cavitation starts, the droplet oscillates in breathing mode, meaning periodic radial movement of liquid inwards and outwards from the droplet centre. Once cavitation starts, the movement of liquid outwards from the centre of the drop cannot be stopped and thus continues to move due to inertia; as a result, the droplet explodes. There is yet another possible explanation for the droplet explosion: boiling in its centre. Such boiling may be a result of dissipation of the initial energy of the acoustically excited drop. The heat deposition is localized in the centre of the droplet, especially when higher acoustic harmonics are developed. Superheating of the droplet may result in the centre temperature exceeding 100 °C and forming a rapidly growing vapour bubble that makes the droplet explode. Narrowing these hypotheses to describe the explosive behaviour of the droplet is a potential future direction of this work.

Our observations of atomization in a variety of liquids seem to confirm one version of the cavitation-wave hypotheses originally laid out by Pohlman and Lierke (Rozenberg, 1973) and Boguslavskii and Éknadiosyants (1969); however, in tissue, no definite mechanism of atomization and tissue erosion has been validated. One possible explanation is that tissue is eroded due to spallation (Maxwell *et al.* 2011, Khokhlova *et al.* 2011a). In other words, the wave reflects upon encountering the pressure release surface, causing significant cavitation just below the tissue surface. As these vapour cavities continue to form, fragments of tissue become separated from the bulk tissue by these cavitation clouds, at which time those fragments move in the direction of the gas. In the ideal case of reflection from the pressure release surface and submicron-size fragments, when the separation is complete, the velocity of the ejected pieces should equal double the particle velocity of the incoming wave. This mechanism would explain why we see whole and fragmented cells and nuclei in the collected projectiles; near the cavitation bubbles, the cells and nuclei could become fragmented due to the shear forces, but in the centre portion of these fragments, the cells would be unaffected. Further experimentation is needed to validate this mechanism.

Upon histological comparison between the fountain projectiles and bulk boiling histotripsy, it was noted that because whole cells and nuclei are still present in the collected projectiles, it differed from the histological analysis of histotripsy and boiling histotripsy in bulk tissue (Parsons *et al.* 2006, Wang *et al.* 2011). We believe the difference may be due to the confined space in the bulk tissue; the length of each ultrasound pulse in addition to the repetition of pulses recirculates the projectiles within the bulk tissue, further fractionating the tissue and breaking up cells. An experiment where the fountain projectiles are recirculated will validate/invalidate this hypothesis and may help determine the number of pulses needed for boiling histotripsy to completely fractionate the cells in bulk tissue.

One further observation made during the tissue studies is that the tissue wetness affects the tissue atomization and erosion rate. Standing liquid on the tissue surface, whether it be phosphate-buffered saline (PBS) or water, substantially enhances atomization and tissue erosion by decreasing the atomization threshold and time for atomization to occur. Blotting the surface to remove the excess liquid from the surface somewhat decreases the atomization and tissue erosion, while not soaking the tissue in PBS at all can almost completely inhibit atomization and tissue erosion. Our current hypothesis is that the thin liquid layer on the

surface makes it easier for the surface capillary waves to form, lowering the cavitation threshold and thereby enhancing atomization and tissue erosion. However, since atomization and erosion are decreased by not soaking the tissue in PBS, it is possible that the PBS alters the tissue structural and the mechanical properties through absorption either in the cells or extracellular matrix. Another alternative is that by not soaking the tissue in PBS the air content of the tissue is increased such that it prevents ultrasound of sufficient intensity to reach the surface, inhibiting atomization. Nevertheless, as increasing the soaking time of liver in PBS increases atomization and tissue erosion, it becomes evident that the process used to prepare tissue or create blood clots can substantially affect the atomization thresholds. Understanding the differences observed during atomization and fountain formation from different tissue preparation methods may help us determine which tissues are candidates for *in vivo* tissue fractionation by boiling histotripsy.

Additionally, erosion rate and atomization threshold are easily affected by local inhomogeneities within the same liver, and even within the same liver sample. While erosion rate and thresholds can be affected by the tissue preparation method as a whole, we found differences in the erosion rates and atomization threshold from site to site. While some of these can be explained by the presence of small vessels and other visible structural inhomogeneities, other variations were not easily elucidated. One explanation may revolve around the small changes in tissue liquid content from site to site; while we attempt to maintain a consistent wetness on the tissue surface, variation at the cellular level may explain some of these discrepancies in the data. The method of liver preparation may also enhance or decrease these subtle differences. Further studies will be performed on tissue preparation techniques and cellular inhomogeneities in tissue to explain these variations.

Already, cavitation cloud histotripsy has been shown to be successful *in vivo* in the canine prostate (Hall *et al.* 2009, Hempel *et al.* 2011) and in the rabbit kidney (Hall *et al.* 2007). Boiling histotripsy has also been shown to successfully emulsify porcine liver and murine melanomas *in vivo* with strong similarities between the *ex vivo* and *in vivo* results (Khokhlova *et al.* 2011b). While the experiments in this paper were conducted in *ex vivo* tissue samples, we expect similar instances of atomization and tissue fractionation when using *in vivo* tissues. The different distribution of gas nuclei in the living tissue may make atomization and tissue erosion less dramatic than has been observed in the *ex vivo* tissue case because it could reduce the intensity of ultrasound reaching the atomization site; however if tissue wetness plays a factor in erosion and atomization, the blood that is present in living tissue might make atomization occur even easier than was found in the *ex vivo* case. Determining the factors that affect atomization and tissue erosion will be important as our work progresses toward *in vivo* studies and as we compare our results to *in vivo* boiling and cavitation cloud histotripsy studies. Furthermore, these factors may be important in predicting the success of boiling histotripsy in many different *in vivo* tissues.

Supplementary Material

Refer to Web version on PubMed Central for supplementary material.

Acknowledgments

This work was supported by the National Institute of Health (DK43881, DK070618, and EB0007643), the National Space Biomedical Research Institute in consortium agreement with the National Aeronautics and Space Administration NCC 9–58, and the Russian Foundation for Basic Research (RFBR 11-02-01189). The authors gratefully acknowledge the help of Drs. Tatiana Khokhlova and Wayne Kreider for fruitful discussions. We also wish to thank the staff and researchers at the Centre for Industrial and Medical Ultrasound (CIMU).

References

Antonevich J. Ultrasonic atomization of liquids. IRE Prof Group Ultrason Eng. 1959; 6:6–15.

Bailey M, Khokhlova V, Sapozhnikov O, Kargl S, Crum L. Physical mechanisms of the therapeutic effect of ultrasound (A review). Acoust Phys. 2003; 49:369–88.

Barreras F, Amaveda H, Lozano A. Transient high-frequency ultrasonic water atomization. Exp Fluids. 2002; 33:405–13.

Bassett J, Bright A. Observations concerning the mechanism of atomisation in an ultrasonic fountain. J Aerosol Sci. 1976; 7:47–51.

Bessonova O, Khokhlova V, Canney M, Bailey M, Crum L. A derating method for therapeutic applications of high intensity focused ultrasound. Acoust Phys. 2010; 56:376–85.

Boguslavskii Y, Éknadiosyants O. Physical mechanism of the acoustic atomization of a liquid. Sov Phys- Acoust. 1969; 15:14–21.

Canney M, Bailey M, Crum L, Khokhlova V, Sapozhnikov O. Acoustic characterization of high intensity focused ultrasound fields: a combined measurement and modeling approach. J Acoust Soc Am. 2008; 124:2406–20. [PubMed: 19062878]

Canney M, Khokhlova V, Bessonova O, Bailey M, Crum L. Shock-induced heating and millisecond boiling in gels and tissue due to high intensity focused ultrasound. Ultrasound Med Bio. 2010a; 36:250–67. [PubMed: 20018433]

Canney M, Khokhlova T, Khokhlova V, Bailey M, Hwang JH, Crum L. Tissue erosion using shock wave heating and millisecond boiling in HIFU fields. ISTU-2009, AIP Conf Proc. 2010b; 1215:36–9.

Éknadiosyants O. Role of cavitation in the process of liquid atomization in an ultrasonic fountain. Sov Phys Acoust. 1968; 14:80–4.

Faraday M. On a peculiar class of acoustical figures: and on certain forms assumed by groups of particles upon vibrating elastic surfaces. Phlios Trans of the Royal Soc of London. 1831; 121:299–340.

Gershenzon E, Éknadiosyants O. The nature of liquid atomization in an ultrasonic fountain. Sov Phys Acoust. 1964; 10:127–32.

Hall T, Hempel C, Wojno K, Xu Z, Cain C, Roberts W. Histotripsy of the prostate: dose effects in a chronic canine model. Urology. 2009; 74:932–7. [PubMed: 19628261]

Hall T, Kieran K, Ives K, Fowlkes B, Cain C, Roberts W. Histotripsy of rabbit renal tissue in vivo: temporal histologic trends. J Endourol. 2007; 21:1159–65. [PubMed: 17949317]

Hempel C, Hall T, Cain C, Fowlkes B, Xu Z, Roberts W. Histotripsy fractionation of prostate tissue: local effects and systemic response in a canine model. J Urol. 2011; 185:1484–9. [PubMed: 21334667]

Il'in B, Éknadiosyants O. Nature of the atomization of liquids in an ultrasonic fountain. Sov Phys Acoust. 1967; 12:269–75.

Il'in B, Éknadiosyants O. Influence of static pressure on the ultrasonic fountain effect in a liquid. Sov Phys Acoust. 1969; 14:452–5.

Kelvin, Lord. Oscillations of a liquid sphere. Math Phys Papers. 1890; 3:384.

Khokhlova T, Canney M, Khokhlova V, Sapozhnikov O, Crum L, Bailey M. Controlled tissue emulsification produced by high intensity focused ultrasound shock waves and millisecond boiling. J Acoust Soc Am. 2011a; 130:3498–510. [PubMed: 22088025]

Khokhlova T, Simon J, Wang Y-N, Khokhlova V, Paun M, Starr F, Kaczkowski P, Crum L, Hwang J, Bailey M. *In vivo* tissue emulsification using millisecond boiling induced by high intensity focused ultrasound. J Acosut Soc Am. 2011b; 129:2477.

Lang R. Ultrasonic atomization of liquids. J Acoust Soc Am. 1962; 34:6–8.

Maxwell A, Wang T, Cain C, Fowlkes J, Sapozhnikov O, Bailey M, Xu Z. Cavitation clouds created by shock scattering from bubbles during histotripsy. J Acoust Soc Am. 2011; 130:1888–98. [PubMed: 21973343]

McCubbin J Jr. The particle size distribution in fog produced by ultrasonic radiation. J Acoust Soc Am. 1953; 25:1013–14.

Nahirnyak V, Yoon S, Holland C. Acousto-mechanical and thermal properties of clotted blood. J Acoust Soc Am. 2006; 119:3766–72. [PubMed: 16838520]

Parsons J, Cain C, Abrams G, Fowlkes J. Pulsed cavitational ultrasound therapy for controlled tissue homogenization. Ultrasound Med Bio. 2006; 32:115–29. [PubMed: 16364803]

Peskin R, Raco R. Ultrasonic atomization of liquids. J Acoust Soc Am. 1963; 35:1378–81.

Rayleigh, Lord. The Theory of Sound. London: Macmillan; 1894.

Rozenberg, L., editor. Physical principles of ultrasonic technology. Vol. 2. New York: Plenum Press; 1973. p. 4-88.

Rozenberg L, Éknadiosyants O. Kinetics of ultrasonic fog formation. Sov Phys Acoust. 1960; 6:369–74.

Silverthorn, D. Human physiology: an integrated approach. 3. Vol. 71–74. San Francisco: Pearson Education Inc; 2004. p. 536-540.

Söllner B. The mechanism of the formation of fogs by ultrasonic waves. Trans Faraday Soc. 1936; 32:1532–6.

Smith NB, Hynynen K. The feasibility of using focused ultrasound for transmyocardial revascularization. Ultrasound Med Bio. 1998; 24:1045–54. [PubMed: 9809638]

ter Haar G. High intensity ultrasound. Semin Laparosc Surg. 2001; 8:77–89. [PubMed: 11337740]

Tjan K, Phillips W. On impulsively generated inviscid axisymmetric surface jets, waves and drops. J Fluid Mech. 2007; 576:377–403.

Tjan K, Phillips W. On the impulsive generation of drops at the interface of two inviscid fluids. Proc R Soc A. 2008; 464:1125–40.

Topp M. Ultrasonic atomization - a photographic study of the mechanism of disintegration. Aerosol Sci. 1973; 4:17–25.

Wang T-Y, Xu Z, Hall T, Fowlkes B, Cain C. An efficient treatment strategy for histotripsy by removing cavitation memory. Ultrasound Med Bio. 2012; 38:753–66. [PubMed: 22402025]

Wang Y-N, Khokhlova T, Canney M, Khokhlova V, Crum L, Bailey M. Histological and biochemical analysis of emulsified lesions in tissue induced by high intensity focused ultrasound. J Acoust Soc Am. 2011; 129:2477.

Wood R, Loomis A. Physical and biological effects of high-frequency sound-waves of great intensity. Philos Mag. 1927; 4:417–36.

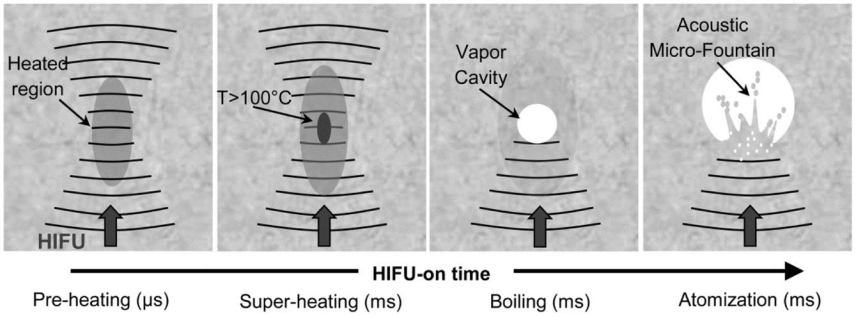

Figure 1.
Proposed mechanism of tissue fractionation by boiling histotripsy.

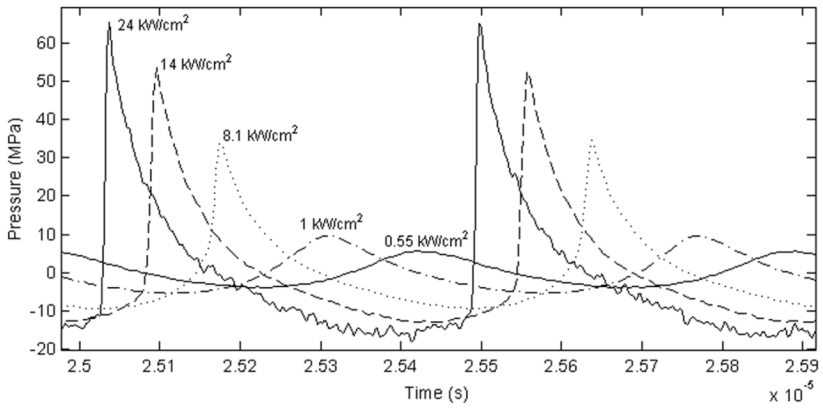

Figure 2.
Waveforms with calculated linear intensities corresponding to experimental conditions for the 2.165 MHz transducer.

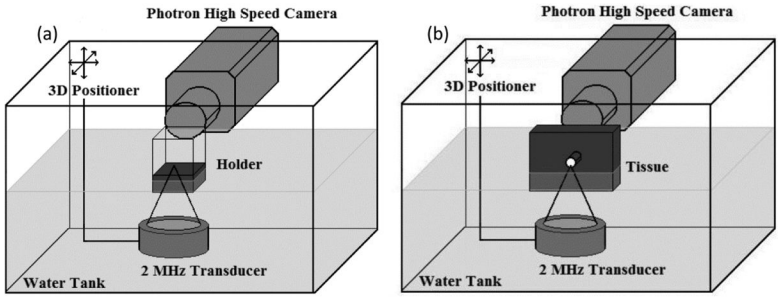

Figure 3.
Macro experimental setups. (a) Shows the planar interface for liquids or tissues in a holder while (b) shows the curved, bubble-like interface for tissue.

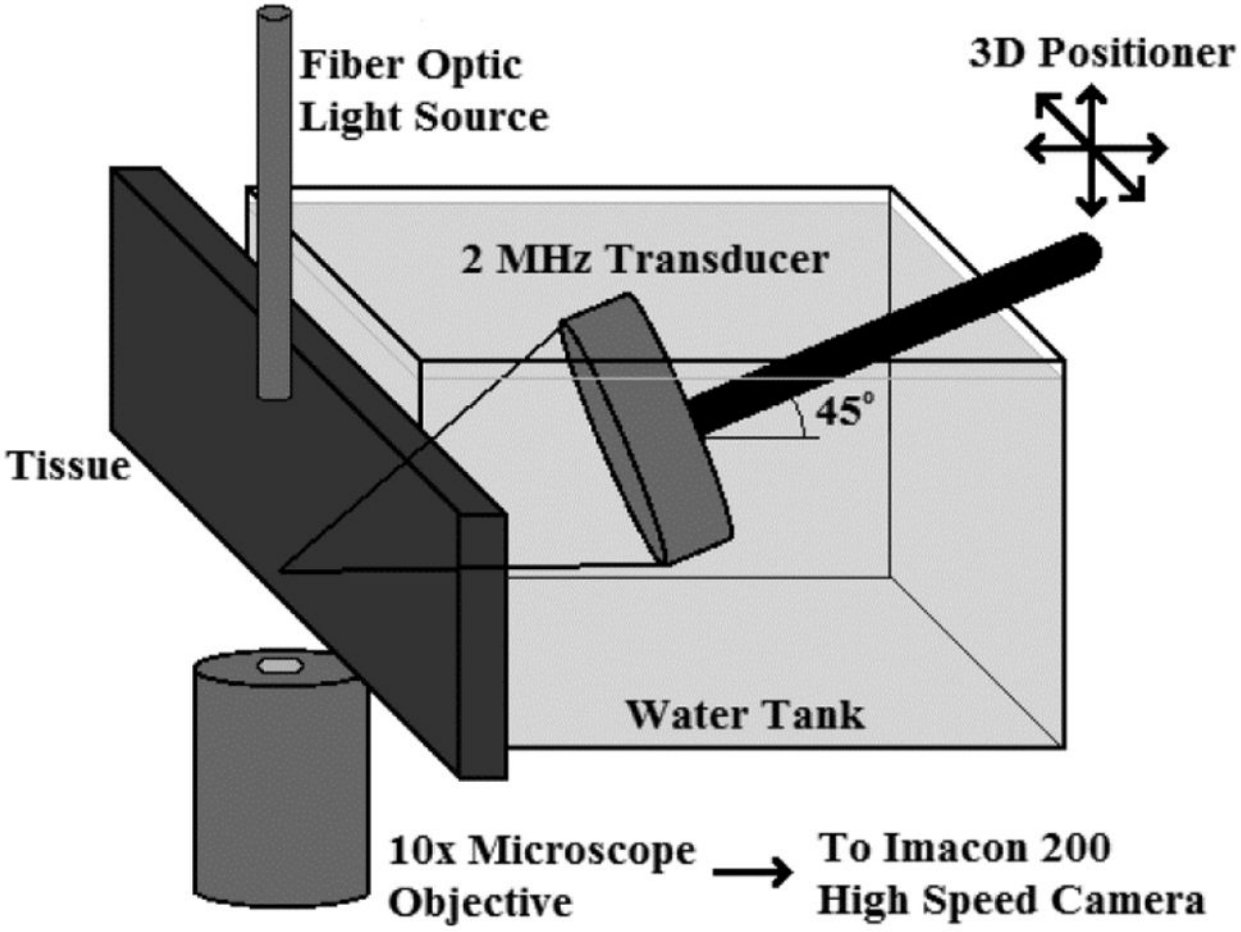

Figure 4.
Micro experimental setup.

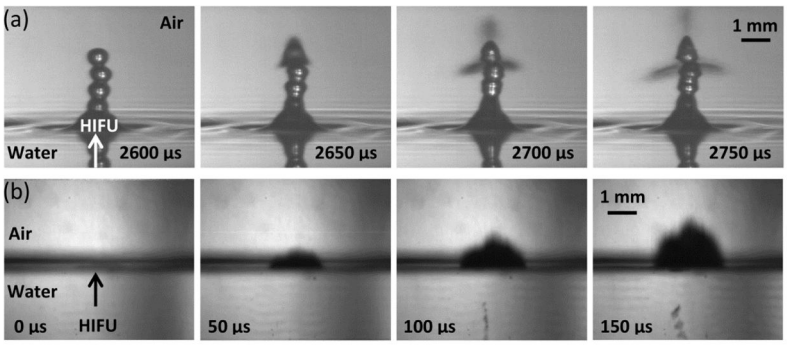

Figure 5.

Air-water interface filmed with (a) the camera lens in air such that the reflections we see in the bottom of the frames are due to an optical reflection of the same jet and (b) the camera lens positioned so that half the objective is facing air and the other half facing water to simultaneously observe effects in water and air. (a) Shows a sequence of images taken at very low intensities (180 W/cm^2) with the camera positioned at a slightly downward angle to catch the surface of the water. Atomization does not occur until the drop chain emerges. At some point, the top drop becomes unstable and atomization jets are released. (b) A sequence of images showing the air to water interface at high acoustic intensities of 24,000 W/cm^2. Cavitation occurs before atomization or jetting and is faintly visible just to the right of the HIFU arrowhead in the first frame, which is taken 20 μs after the acoustic wave arrives at the water surface. As the ultrasonic pulse continues, the cavitation bubbles just below the water surface are joined by a cavitation bubble cloud further below the surface, possibly due to the standing wave pattern that develops upon the reflection of the acoustic wave. In both cases, the total HIFU-on time was 10 ms. This figure is available in movie form in supplement 1.

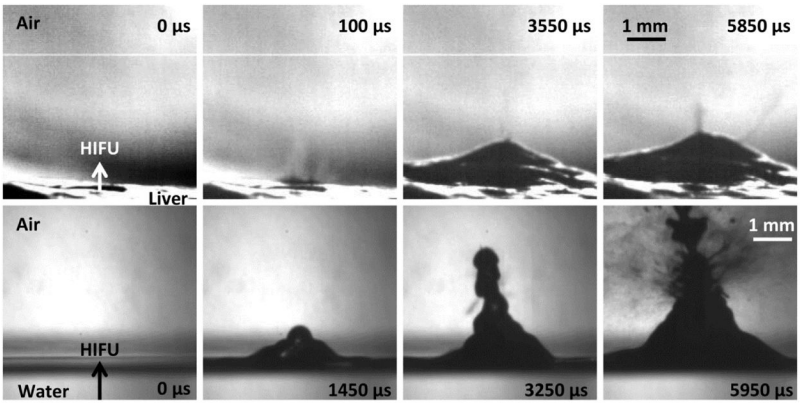

Figure 6.

A direct comparison of liver (upper) and water (lower) at intensities slightly above their respective atomization thresholds (8100 W/cm^2 derated for liver and 550 W/cm^2 for water). In both cases, the first frame occurs 20 μs after the ultrasonic wave arrives at the interface. The second shows the initial spray of atomization in liver (upper) and the mound forming in water (lower) with no atomization. The third frame shows the small spray of atomization from the mound in liver and the first case of atomization for water; whereas the final frame shows atomization at its most significant. The timing is fairly similar between liver and water; the only difference is that liver has that first initial spray of atomization before the mound forms and enhances atomization, while at this intensity water forms the mound before atomization occurs. In both cases, the total HIFU-on time was 10 ms. This figure is available as a movie in supplement 2.

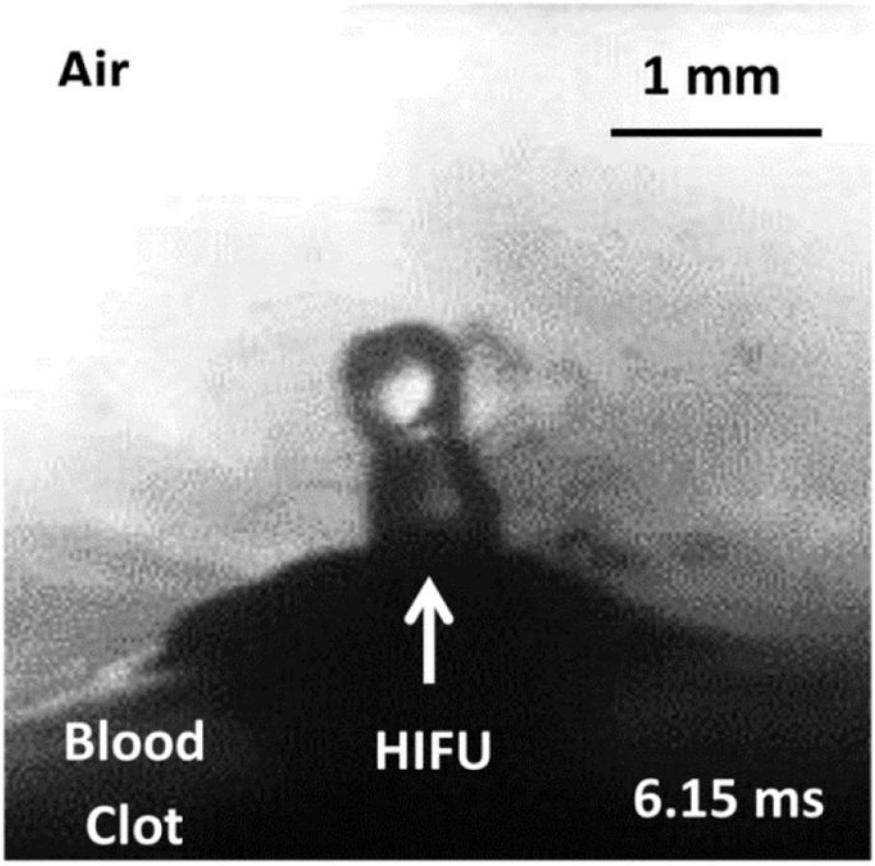

Figure 7.
A drop-chain fountain emerging from the surface of a blood clot at 1000 W/cm^2, derated, an intensity just above the atomization threshold in blood clots. In this case, the total HIFU-on time was 10 ms.

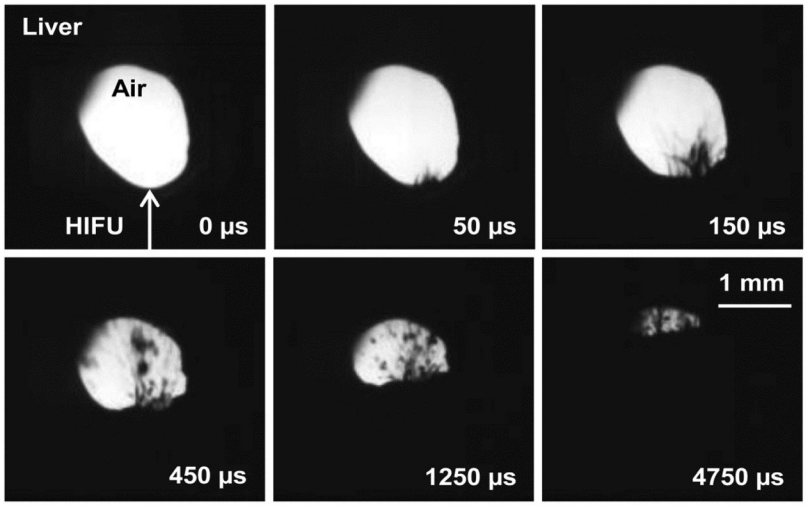

Figure 8.
Cylindrical, bubble-like tunnel through bovine liver at linear intensity of 14,000 W/cm^2, derated. At this intensity, there is a spurt of atomization that becomes more pronounced as the mound forms in the tissue. After around 5 ms, the hole becomes occluded with the spray. In this case, the total HIFU-on time was 10 ms. This movie is available in supplement 4.

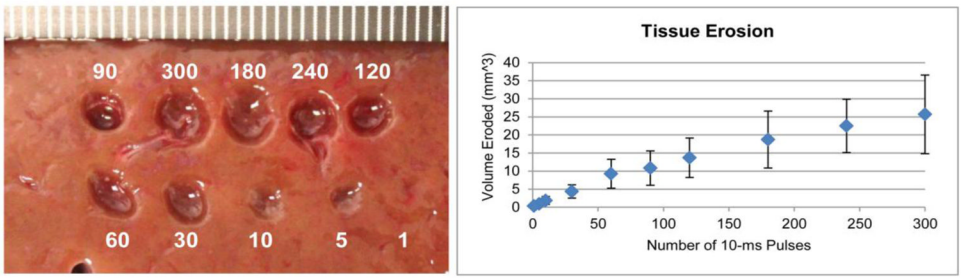

Figure 9.

Left: Tissue erosion observed on the surface of bovine liver at the maximum acoustic intensities of 14,000 W/cm^2, derated, after a varying number of 10-ms pulses all at 1 Hz PRF. Right: A plot of the overall tissue erosion plotted as volume eroded per number of 10-ms pulses.

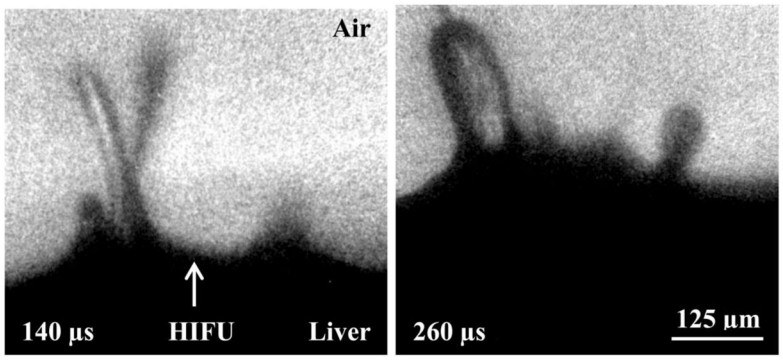

Figure 10.
Magnified jets emitted from the surface of bovine liver. The jet(s) on the left side of each frame begin as thin streams and thicken over time. The jet on the right side of each frame shows how jets often start as the emission of a fog before developing into more significant jets. Furthermore, the right frame shows more jets forming between the established jets. The total HIFU-on time was 10-ms.

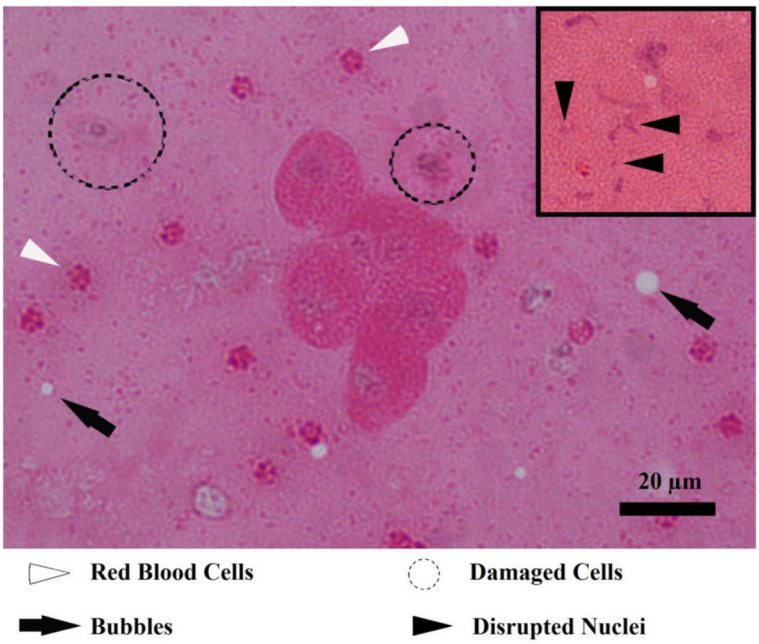

Figure 11.
H&E stain of the collected fountain projectiles. In the centre of the image, a cell cluster consisting of six whole cells is present. In addition, there are red blood cells (white arrowheads), damaged or dying cells (dotted circles), and vapour bubbles (black arrows). The insert shows smeared and fragmented nuclei (black arrowheads).

Table 1

Summary of atomization and fountain results for 6 materials[a]

Material	Threshold Intensity	Max Mound Width at Base[b]	Time to Atomize	Fountain Height	Jet Velocities
Water	350 W/cm^2	4.0 mm	2 μs	< 1 mm	11m/s
Castor Oil	NA	8.5 mm			
Glycerol	NA	8.6 mm			
70% Ethanol	180 W/cm^2	3.1 mm	~μs	< 1 mm	25 m/s
Blood Clot	250 W/cm^2,[c]	3.2 mm	> 20 μs	1.5 mm	10 m/s
Liver	6200 W/cm^2,[c]	5.5 mm	20μs	1 mm	13 m/s

[a] Unless otherwise specified, results are for the maximum acoustic intensity (24,000 W/cm^2) and 1 10-ms pulse

[b] Base width measured at threshold intensity

[c] *In situ* intensity